

On the extraction of extended structure from Herschel-SPIRE scanning observations in the presence of $1/f$ noise

B. Sibthorpe,^{1,2*} P. Chaniai,³ T. J. Waskett¹ and M. J. Griffin¹

¹*School of Physics and Astronomy, Cardiff University, Queens Buildings, The Parade, Cardiff CF24 3AA*

²*UK Astronomy Technology Centre, Royal Observatory, Blackford Hill, Edinburgh EH9 3HJ*

³*Physics Department, Imperial College London, South Kensington Campus, London SW7 2AZ*

Accepted 2008 May 26. Received 2008 May 26; in original form 2006 November 23

ABSTRACT

We present results from a study of the impact of uncorrelated $1/f$ noise on the extraction of spatial structure, on a range of scales, from sky mapping observations made using the Herschel-SPIRE (the spectral and photometric imaging receiver) photometer in the scan-map mode. These studies were carried out using a detailed instrument simulator, and the output reduced using the map-making algorithm to be implemented in the SPIRE data pipeline. The influence of source size scale, telescope-scanning rate and $1/f$ noise knee frequency is investigated, and operational bounds to the expected losses are presented, using the case of zero $1/f$ (white) noise as a benchmark. Both cross-linked and non-cross-linked observing options are studied. The results presented here represent the best current estimate of the sensitivity of the SPIRE photometer to emission on arbitrary scales. The data presented are general and scalable to any SPIRE observation made using the scanning mode.

Key words: instrumentation: miscellaneous – methods: observational – methods: statistical – space vehicles: instruments – infrared: general – submillimetre.

1 INTRODUCTION

SPIRE, the spectral and photometric imaging receiver (Griffin et al. 2006), is one of three instruments onboard the European Space Agency's (ESA) Herschel Space Observatory (Pilbratt 2005). Like a number of other new instruments operating at far-infrared (FIR) and submillimetre (submm) wavelengths, it is designed to carry out large area imaging surveys. The primary SPIRE observing mode for such surveys is 'scan-map', which operates without the need to chop. As a result, it is also susceptible to $1/f$ noise, so called as its power spectrum has an inverse relationship with frequency. Consequently, there is greater power at low frequencies resulting in long time-scale noise drifts. This makes the accurate recovery of the sky brightness distribution on large spatial scales a particularly difficult observational challenge.

In scanning observations, sky structure on different spatial scales is encoded at different electrical frequencies in the detector output, with larger scales corresponding to lower frequencies. In principle, it is desirable to be able to characterize structure on arbitrarily large scales; in practice, there will be some limit on the size scale imposed by the overall $1/f$ noise and the scan rate. Targets with such a large-scale structure include diffuse emission from Galactic star-

forming clouds, circumstellar dust shells, cirrus clouds and nearby galaxies.

It is important to understand the limitations on the recovery of the sky brightness distribution imposed by $1/f$ noise to ensure that the observing modes and integration times are optimised and that the analysis methods to be used are well matched to the data. A thorough understanding of the expected signal-to-noise ratio (SNR) from an observation of such a diffuse region is also important in the planning of specific science programmes. This is particularly important for satellite instruments, for which observing time is costly and the in-flight time available for the performance verification and optimisation is limited.

In this paper, we derive a quantitative estimate for the sensitivity of the SPIRE photometer to extended structure, when operating in the scan-map mode. The studies are performed using a detailed instrument simulator, whose output is then reduced using the maximum-likelihood map-making algorithm to be implemented in the SPIRE data pipeline. Simulations are performed using the optimal cross-linked scan-map strategy (Waskett et al. 2007), and compared to a non-cross-linked strategy.

Finally, we apply the sensitivity estimates to the specific case of compact sources and attempt to determine how the simultaneous presence of $1/f$ noise and diffuse cirrus limits their detection.

In Section 2, we briefly review the SPIRE instrument, its observing modes, sources of error and efforts to simulate its data. Section 3 outlines the simulations performed to investigate the effect of $1/f$

*E-mail: sib@roe.ac.uk

noise and Section 4 presents the results from these simulations. Finally, Section 5 summarizes the findings of these investigations.

2 THE HERSCHEL-SPIRE INSTRUMENT

SPIRE contains a three-band submm camera and an imaging Fourier transform spectrometer (FTS), and uses arrays of hexagonally packed feedhorn-coupled bolometric detectors operating at a temperature of 300 mK. The photometer has a field of view (FoV) of 4×8 arcmin², observed simultaneously in spectral bands centred approximately at 250, 360 and 520 μm . The angular resolution is determined by the telescope diffraction limit, with full width at half-maximum (FWHM) beamwidths of approximately 18, 25 and 36 arcsec at 250, 350 and 500 μm , respectively. Maximizing the aperture efficiency of the feedhorns requires an aperture corresponding to an angle of $2\lambda/D$ on the sky, where λ is the wavelength and D is the telescope diameter. Consequently, the detector beams have an angular separation of approximately twice the FWHM beam size on the sky. As a result, specific observing patterns – either jiggling or scanning – must be employed to achieve Nyquist sampling of the sky brightness distribution (Griffin, Bock & Gear 2002).

The layout of the SPIRE photometer arrays is shown schematically in Fig. 1. The arrays have the same FoV on the sky but are shown separately here for clarity. There are 139, 88 and 43 detectors in the 250, 350 and 500 μm arrays, respectively. There are also two ‘dark pixels’, bolometers positioned outside the instrument FoV and two thermistors located on each array.

2.1 The SPIRE map-making algorithm

SPIRE will use an implementation of the maximum-likelihood map-making algorithm MADmap (Cantalupo 2002) in the standard data reduction pipeline. This type of algorithm makes use of the redundant information from cross-linked observations to establish a noise covariance matrix. It is then used to effectively down weight the contribution from $1/f$ noise, thus reducing the $1/f$ noise in the map (Tegmark 1997). Greater levels of cross-linking will enable a maximum-likelihood map-maker to operate more effectively

(Tegmark 1997). As a result, this method is dependent on the observing strategy used.

This method is widely used by cosmic microwave background (CMB) experimenters (Poutanen et al. 2006). If cross-linked observations are not performed, then the output from this algorithm will be a naive map (i.e. a map in which each pixel value is equal to the average value of all of the measurements falling within the pixel area) as this is the optimal map reconstruction for data obtained via a non-cross-linked scanning strategy.

2.2 Observing modes

The SPIRE photometer has three main observing modes: point source photometry, field (jiggle) mapping and scan mapping (Griffin et al. 2006). In this paper, we deal solely with the latter, which is used for maps significantly larger than the SPIRE FoV. For SPIRE, scanning is the preferred operating mode for large-area surveys as it provides a larger instantaneous FoV, improved sensitivity and the ability to recover extended structure.

When operating in the scan-map mode, the detector array must be at a suitable angle with respect to the scan direction to fully sample the sky in a single observation. An angle of $42^\circ 4'$ was found to provide a highly uniform coverage map while maintaining an acceptable level of redundancy in the data (Sibthorpe, Waskett & Griffin 2006).

Constraints imposed by the spacecraft mean that Herschel cannot perform curved scans. This rules out complicated observing strategies such as the Lissajous curves employed by SHARC-II (The SHARC-II Homepage – www.submm.caltech.edu/~sharc/). The time required to change scan direction with the Herschel telescope means that the Pong strategy, implemented by SCUBA-2 (Holland et al. 2006), is also ruled out due to poor observing efficiency. Therefore, the nominal SPIRE observing strategy is a simple raster scan, also known as ‘on the fly’ scanning, as seen in Fig. 2.

Two or more cross-linked raster maps must be performed, at relative angles of not less than 20° (Waskett et al. 2007), to provide sufficient redundant information for the maximum-likelihood map-maker to produce an optimal map. The limitation in scanning angles available with SPIRE means that a cross-linked angle of $84^\circ 8'$ must be used (Waskett et al. 2007). The largest cross-linked map that can be performed by Herschel is a square with sides of 4° (Herschel-Spot Users’ Guide 2007).

The nominal telescope-scan rate is 30 arcsec per second and can be up to 60 arcsec per second. Should $1/f$ noise be significant, additional chopping motion can be added using the internal beam steering mirror to introduce a higher frequency signal modulation;

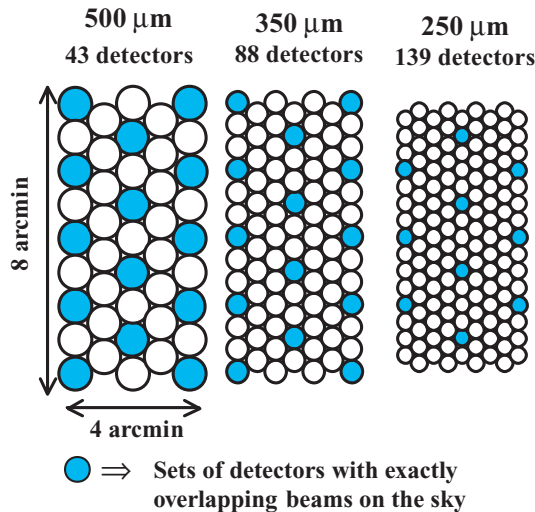


Figure 1. Schematic of SPIRE photometer arrays. The circles represent the feedhorn openings for each detector, and the shaded circles represent co-aligned pixels.

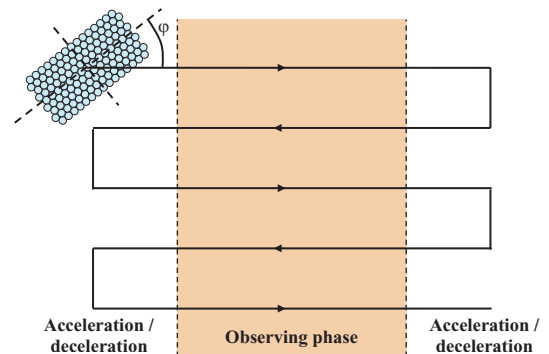


Figure 2. Raster scan pattern as implemented by Herschel-SPIRE.

however that is not expected to be used, and will not be supported in the initial data pipeline.

2.3 Sources of noise and error

The SPIRE detectors and electronics are designed to ensure that the instrument is photon noise limited. As with any physical system however, additional noise will occur at low frequencies, resulting in a $1/f$ -type noise power spectrum which approaches the white noise level at high frequencies. The $1/f$ noise can be characterized by the white noise level, the index of the $1/f$ noise and the $1/f$ knee frequency, f_k , defined as the frequency at which the noise power spectrum is twice that of the white noise level. Low values of f_k are desirable as this corresponds to fluctuations on longer time-scales, and hence to a more stable observing system.

In the case of SPIRE or similar scanning photometric instruments operating in the FIR, there are a number of sources of $1/f$ noise that may contribute to the overall noise level. There will be a $1/f$ noise component unique and specific to each detector in an array. This noise arises from uncorrelated physical processes in the detectors and electronic components, therefore the noise time-lines are not correlated from one detector to another. In this case, the $1/f$ originates from the Johnson noise in the detector and the associated load resistor. As a result, the index of the power spectrum is expected to be -1 .

Common mode $1/f$ noise is shared by detectors within a single array. In SPIRE, the dominant source of common mode $1/f$ noise is expected to be thermal fluctuations in the bath temperature provided by the fridge. These fluctuations will be experienced simultaneously by all detectors in an array, assuming that the thermal impedance between the cooler cold tip and the individual detector is uniform. Even in that case, the effects on the individual detector outputs may be different depending on the specific detector parameters. In order to minimize the thermal fluctuations arriving at the detector arrays, a photometer thermal control system is implemented. This monitors the temperature of the arrays, and adjusts power to a heating element within the detector assembly in an attempt to keep the array temperature near constant.

Any residual thermal fluctuations which do occur within a detector array are tracked by thermometers and dark pixels mounted on the array. This information is then used by the data pipeline to remove their influence on the output data. The process of correlated noise removal will not be 100 per cent efficient however, and there is expected to be some residual correlated $1/f$ noise in the output time-line. Recent analysis of SPIRE test data has shown that the data, both before and after correlated noise removal, have the same spectral index of ~ -1 . Before the removal of the correlated $1/f$ noise, the $1/f$ knee frequency is near the requirement value of ~ 100 mHz. This drops to the nominal value of ~ 30 mHz after the removal of the correlated noise. After this stage in the data pipeline, any residual-correlated $1/f$ noise will be dealt with as though it were uncorrelated by the map-making algorithm MADmap.

2.4 The SPIRE photometer simulator

Two software simulators have been developed for SPIRE, one for the photometer and one for the FTS. For information on the FTS simulator programme refer to Lindner, Naylor & Swinyard (2004). The photometer simulator (Sibthorpe et al. 2004) is designed to be a detailed and flexible computer representation of the entire photometer system, taking into account both telescope and instrument elements.

The primary functions of the photometer simulator are as follows.

- (i) Generation of realistic data streams to aid in the development and testing of data analysis software.
- (ii) Analysis of systematic effects on specific science cases.
- (iii) Identification of the most suitable observing mode for a given science case, and optimisation of the corresponding observing mode parameters.

Realistic data streams can be generated for all primary observing modes via ‘observation’ of an artificial sky with the simulated instrument. This allows the operating modes and data reduction software to be tested, and instrument systematics to be diagnosed and evaluated. In addition to sampled data and housekeeping time-lines, other time-lines, unobtainable in the physical system, such as noiseless detector outputs, are available for analysis, allowing the complete system performance to be scrutinized. Simulator data can be reduced using either SPIRE data reduction software or routines specifically developed for the analysis of simulator output. The basic sensitivity levels that SPIRE is expected to achieve have been estimated using a photometric model of the instrument (Griffin et al. 2006); however the simulator constitutes a more sophisticated and versatile tool for evaluating the photometer performance and how it is affected by the specific observing mode parameters. It will also be used as a diagnostic tool for the instrument behaviour both in ground testing and in flight operation.

3 SIMULATIONS

The degradation of SNR due to $1/f$ noise depends on the $1/f$ knee frequency, f_k , the telescope-scan rate, $\dot{\theta}$, and the beam-convolved source size scale, λ . The index of the $1/f$ noise is also important, however in this case we know from SPIRE test data that the index is ~ -1 (see Section 2.3).

Together, f_k and $\dot{\theta}$ determine the spatial frequency scale in the map corresponding to the $1/f$ knee spatial frequency ($f_s = f_k/\dot{\theta}$). The equivalent angular size scale is $\lambda_s = 1/f_s$. Crudely, the SNR of a source close to or greater than this scale, observed in the presence of $1/f$ noise, will be significantly reduced.

It is convenient to define a new variable, ψ , in the following way:

$$\psi = \frac{f_k \lambda}{\dot{\theta}}. \quad (1)$$

This combines all the information from the three related variables into a single dimensionless parameter, ψ .

The impact of $1/f$ noise is influenced by all three parameters, and identical values of ψ can be achieved for a range of source scales, and scan rates, given a constant $1/f$ knee frequency. A single scalable plot can be derived which is capable of representing any combination of the dependent parameters.

A series of simulations was performed in order to characterize the impact of the $1/f$ noise. Simulations were performed using a range of f_k , $\dot{\theta}$ and λ values. The values chosen equate to a ψ range of 0–8, equivalent to an observation of the maximum cross-linked map size (4°), at the fastest scanning rate, and for the nominal $1/f$ knee frequency.

The SPIRE scan-map mode without chopping was used for all simulations. In order to establish the fundamental limits on data quality imposed by unavoidable $1/f$ noise from the detectors themselves, various simplifications were introduced: no common mode noise or pointing errors were included; the detectors in a given array were taken to be identical (perfect flat-fielding) and there were no correlated thermal drifts, cross-talk or glitches. Whilst these

conditions are not fully representative of the real system performance, they do allow us to investigate the consequence of residual $1/f$ noise alone. Other noise effects may also reduce the data quality, but these will act as a scaling upon the white noise level, and hence will not impact the results presented here.

The noise time-line imposed on each detector was unique, but generated using the same noise spectrum (noise voltage spectral density, f_k , and index). This represents uncorrelated noise within each detector channel arising from independent detectors and their readouts.

The simulated cross-linked and non-cross-linked time ordered data were converted to a map using MADmap, as implemented in the SPIRE data pipeline.

The $1/f$ noise level at a particular source size scale was measured from the noise power spectrum, and normalized to the white noise level. The effective relative sensitivity (ERS) was then derived relative to the white noise case. This is a measure of the change in sensitivity due to $1/f$ noise as a factor of the white noise level, and is defined as

$$\text{ERS} = \frac{\sigma_w}{\sigma_\psi}, \quad (2)$$

where σ_w is the white noise level in the map and σ_ψ is the noise in the map in the presence of $1/f$ noise. This allows us to quantify the sensitivity degradation due to $1/f$ noise, independent of the integration time and integrated source flux.

4 RESULTS

The ERS as a function of $1/f$ knee frequency is illustrated in Fig. 3, for the sample beam-convolved size scale of 25 arcsec, equivalent to a point source observed in the SPIRE 350 μm band, and nominal telescope-scan rate. This figure shows the result for both the cross-linked and non-cross-linked cases. The loss in sensitivity with increased f_k is more rapid in the non-cross-linked compared to the cross-linked case; the ERS drops to 0.85 in the non-cross-linked case, as opposed to 0.95 in the cross-linked case, for the f_k requirement of 100 mHz.

The ERS for all scales, plotted as a function of ψ , is presented in Fig. 4 for both scanning strategies. When plotted in this way, the data from all of the source scales and $1/f$ knee frequencies lie on approximately the same line.

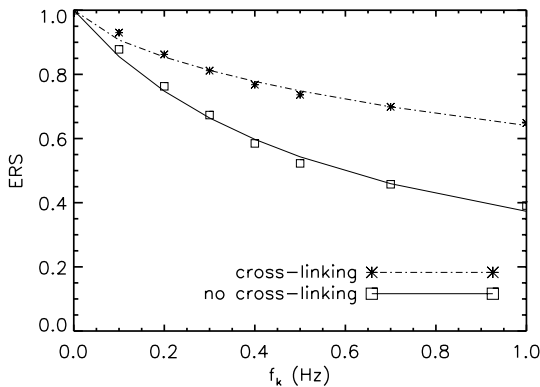


Figure 3. ERS as a function of f_k for the observation of a point source in the SPIRE 350 μm band. This equates to a 25 arcsec beam-convolved source size scale. The scan was made at the nominal scanning rate of 30 arcsec per second. The ERS for both the cross-linked and non-cross-linked cases is shown.

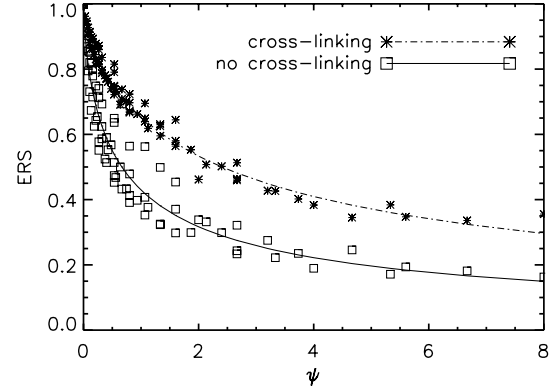


Figure 4. Variation of ERS as a function of ψ for cross-linked and non-cross-linked observing strategies.

The lines fitted to both sets of data in Fig. 4 provide a general result, and have the empirically derived functional form:

$$\text{ERS} = \frac{1}{1 + a\psi^b} = \frac{1}{1 + a(f_k\lambda/\dot{\theta})^b}, \quad (3)$$

where a and b are 0.53 and 0.72 for the cross-linked case and 1.33 and 0.70 for the non-cross-linked case, respectively.

Using these equations, the ERS can be calculated for a range of source size scales, telescope scanning rates and $1/f$ noise knee frequencies, when observing with either scanning strategy. In cases where many repeat observations are performed, any additional cross-linking at different angles can be expected to provide a minor improvement to the ERS as a function of ψ . In these cases, the result presented here should be regarded as a lower limit.

In order to demonstrate the benefit of using the cross-linked strategy over the non-cross-linked strategy, consider an example situation: we want to determine the largest source scale observable whose ERS is not below 0.7, given the nominal SPIRE scanning rate and nominal $1/f$ knee frequency. Under these circumstances, the maximum source scale in the non-cross-linked case is ~ 3.3 arcmin, whereas the cross-linked case is nearly four times the size at ~ 12.4 arcmin.

A further example is shown in Table 1, where the ERS is presented for point source observations (i.e. λ equal to the beam size) in each band. The table contains values for both the nominal and required values of f_k . The ERS is higher in all cross-linked cases compared to non-cross-linked cases further demonstrating the benefits of this method.

The results presented in this paper are most applicable to sources with scales greater than a beam, and sources whose structure is

Table 1. ERS in the non-cross-linked and cross-linked cases for scan-map observations of point sources in the three SPIRE photometer bands. Values for both the required and nominal $1/f$ knee frequencies are presented for the nominal telescope-scan rate ($\dot{\theta} = 30$ arcsec per second).

f_k (mHz)	Band (μm)	ERS	
		non-cross-linked case	cross-linked case
100 (requirement)	250	0.84	0.93
	350	0.81	0.91
	500	0.77	0.90
30 (nominal)	250	0.92	0.97
	350	0.91	0.96
	500	0.88	0.95

not previously well known. Observations of point sources will produce features of known size and structure (i.e. a beam shape) in their output maps. Analysis methods such as matched filtering and Fourier filtering can use this information to increase the effective sensitivity to these sources. Consequently, the results in Table 1 can be considered a lower limit to the sensitivity of SPIRE to point sources.

4.1 Observing time calculation

It is important to use the ERS when planning the time required for an observation, as it ensures that the desired instrumental noise level, averaged over the length of an observation, is reached. In the pure white noise case, an instrumental noise level of σ_w can be reached in time t_w . However, in the presence of $1/f$ noise, the true noise level reached after t_w will be a factor of σ_w/ERS higher. To reach the original desired noise level, σ_w , in the presence of $1/f$ noise, will take a time $t_\psi = t_w(\sigma_w/\text{ERS})^2$; a factor of $(\sigma_w/\text{ERS})^2$ longer.

Take as an example the observation of a Gaussian source with FWHM equal to that of the SPIRE 500 μm beam. This equates to a convolved source size scale of ~ 50 arcsec in the 500 μm band, and corresponds to an ERS of 0.94, and 0.86, for the cross-linked, and non-cross-linked cases, respectively, when scanning at the nominal scan rate with the nominal $1/f$ knee frequency. If the desired instrument rms white noise level for this observation is σ_w , then the instrumental noise including $1/f$ noise (σ_ψ) will be σ_w/ERS . Therefore, an observation must be a factor of $(\sigma_w/\text{ERS})^2$ longer to achieve a SNR equivalent to that which would be achieved in the white noise case. For a source of the size described above, the integration time would increase by a factor of 1.13 in the cross-linked case and by a factor of 1.35 in the non-cross-linked case.

5 CONCLUSION

In this paper, we have performed a series of investigations into the impact of $1/f$ noise when observing with the SPIRE photometer in the scan-map mode. The investigation studied the effect of three interdependent parameters: $1/f$ knee frequency, scanning rate and convolved source size scale. The results are general and represent the realistic limits to the sensitivity of SPIRE when observing sources of an arbitrary scale. While there are other possible systematic effects, it is likely that these will act as a scaling on the total instrumental noise which has been normalized out in this study.

The maps used in this analysis were generated from simulated cross-linked and non-cross-linked observation data using the MADmap algorithm, as implemented in the SPIRE data pipeline. This was to produce an output which matches as closely as possible the expected in-flight SPIRE performance. The ERS was plotted for both scanning strategies as a function of ψ , a dimensionless parameter which combines all three of the investigated variables. A fit was made to both sets of data to produce general results for both cases. A comparison of the ERS derived from both scanning options showed the cross-linked case to be superior in all situations

where $f_k \neq 0$, with the most significant improvement being found for large values of ψ .

The general results for both cases can be used to estimate the instrumental noise for a particular size scale, as a factor of the theoretical white noise, for a given $1/f$ noise knee frequency and telescope-scan rate. This allows for more accurate calculation of observing times. It should be noted that the results presented here for the cross-linked case are applicable only to the optimal SPIRE observing strategy (Waskett et al. 2007).

The results outlined are important in the planning of large-scale observing programmes in which both extended and compact sources are required to be observed simultaneously. They allow for an informed selection of scanning speed to ensure that the source scales of interest are observed efficiently, and provide information on the integration times required to ensure that the desired detection limits are reached.

ACKNOWLEDGMENTS

The authors acknowledge the UK Science and Technology Facilities Council (STFC) for a research studentship and postdoctoral funding. We would also like to thank the referee, Attila Kovacs, for his invaluable help and input to this paper.

REFERENCES

- Cantalupo C., 2002, MADmap: A Fast Parallel Maximum Likelihood CMB Map Making Code. Available at: <http://crd.lbl.gov/cmc/MADmap/doc/>
- Griffin M. J., Bock J. J., Gear W. K., 2002, *Appl. Opt.*, 41, 6543
- Griffin M. et al., 2006, in Mather J. C., MacEwen H. A., de Graauw M. W. M., eds, *Proc. SPIE Vol. 6265, Space Telescopes and Instrumentation I: Optical, Infrared, and Millimeter*. SPIE, Bellingham, p. 7
- Herschel-Spot Users' Guide, 2007, Herschel-Spot (HSpot) Users' Guide: Herschel Observation Planning Tool. Available at: http://herschel.esac.esa.int/Docs/HSPOT/html/hspot_om.html
- Holland W. et al., 2006, in Zmuidzinas J., Holland W. S., Withington S., Duncan W. D., eds, *Proc. SPIE Vol. 6275, Millimeter and Submillimeter Detectors and Instrumentation for Astronomy III*. SPIE, Bellingham, p. 45
- Lindner J. V., Naylor D. A., Swinyard B. M., 2004, in Mather J. C., ed., *Proc. SPIE Vol. 5487*, p. 469
- Pilbratt G. L., 2005, in Wilson A., ed., *ESA SP-577, Proc. Dusty and Molecular Universe*. ESA, Noordwijk, p. 3
- Poutanen T. et al., 2006, *A&A*, 449, 1311
- Sibthorpe B., Woodcraft A. L., Griffin M. J., Watkin S. L., 2004, in Mather J. C., ed., *Proc. SPIE Vol. 5487, Optical, Infrared, and Millimeter Space Telescopes*. SPIE, Bellingham, p. 491
- Sibthorpe B., Waskett T. J., Griffin M. J., 2006, in Silva D. R., Doxsey R. E., eds, *Proc. SPIE Vol. 6270, Observatory Observations: Strategies, Processes and Systems*. SPIE, Bellingham, p. 41
- Tegmark M., 1997, *Phys. Rev. D*, 56, 4514
- Waskett T. J., Sibthorpe B., Griffin M. J., Chanial P. F., 2007, *MNRAS*, 381, 1583

This paper has been typeset from a $\text{\TeX}/\text{\LaTeX}$ file prepared by the author.